



Virginia Commonwealth University
VCU Scholars Compass

Theses and Dissertations


Graduate School

2021

Equations of State for Warm Dense Carbon from Quantum ESPRESSO

Derek J. Schauss
Virginia Commonwealth University

Follow this and additional works at: <https://scholarscompass.vcu.edu/etd>

 Part of the [Atomic, Molecular and Optical Physics Commons](#), [Computer Sciences Commons](#), [Condensed Matter Physics Commons](#), [Materials Science and Engineering Commons](#), [Mechanical Engineering Commons](#), [Nuclear Commons](#), [Nuclear Engineering Commons](#), [Plasma and Beam Physics Commons](#), and the [Quantum Physics Commons](#)

© The Author

Downloaded from

<https://scholarscompass.vcu.edu/etd/6702>

This Thesis is brought to you for free and open access by the Graduate School at VCU Scholars Compass. It has been accepted for inclusion in Theses and Dissertations by an authorized administrator of VCU Scholars Compass. For more information, please contact libcompass@vcu.edu.

Equations of State for Warm Dense Carbon from Quantum ESPRESSO

By

Derek Schauss

May 14, 2021

Thesis

Submitted for the fulfillment of

Master Degree in Nuclear and Mechanical Engineering

For Virginia Commonwealth University

Richmond, Virginia

Advisor:

Dr. Gennady Miloshevsky

Acknowledgments

First and foremost, I would like to thank Dr. Gennady Miloshevsky for welcoming me into his research group. This kind act paired with his constant patience and answers to my countless questions made this thesis possible, and it certainly would not exist without him. Prior to meeting him, I never thought that I would publish a research paper or write another thesis, so thank you, Professor, for giving me this chance and for everything else along the way.

Secondly, I must thank Dr. Karla Mossi and Dr. June Wicks, the other members of my committee. Dr. Mossi's help extends back to before my acceptance into VCU was even official, and for it I am duly grateful. The number of administrative and miscellaneous questions I asked Dr. Mossi is comparable to the technical ones I posed to Dr. Miloshevsky, so thank you for your patience and consistent help as well. June, thank you for taking the time out of your schedule to aid in the completion of this thesis. It was a pleasure to meet and conduct research with you.

Finally, I would like to recognize Mrs. Dena Moore; her kind advice led to my connections with Dr. Mossi and, eventually, Dr. Miloshevsky. Without ever meeting me, she went above and beyond for someone she knew only as a friend of her son. Mrs. Moore, thank you for your wise and selfless counsel. May I have the chance to pay it forward one day!

To my parents and the good Lord above, let me express my utmost gratitude for the patience and calm insistence that, given time, everything falls into place. Thank you.

This research is sponsored by the Defense Threat Reduction Agency, Grant No. DTRA1-19-1-0019.

Abstract

Warm dense plasma is the matter that exists, roughly, in the range of 10,000 to 10,000,000 Kelvin and has solid-like densities, typically between 0.1 and 10 grams per centimeter. Warm dense fluids like hydrogen, helium, and carbon are believed to make up the interiors of many planets, white dwarfs, and other stars in our universe. The existence of warm dense matter (WDM) on Earth, however, is very rare, as it can only be created with high-energy sources like a nuclear explosion. In such an event, theoretical and computational models that accurately predict the response of certain materials are thus very important. Unfortunately, given both the impracticality of producing WDM on Earth and the inherent complexity of the matter itself (partial ionization, non-negligible electron-nuclei interactions, etc.), modeling WDM has proved strenuous and problematic. Despite this difficulty and complexity, advances in Density Functional Theory Molecular Dynamics (DFT-MD) have made such simulations possible. In this thesis, elemental carbon was modeled because of its low atomic number and its relative abundance of experimental data. The Car-Parrinello MD package implemented in the code Quantum ESPRESSO was used to simulate warm dense carbon. Carbon cells were comprised of 24 atoms assigned random positions and were modeled at densities typical of WDM. System temperature was set with the Nosé-Hoover thermostat and by rescaling ionic velocities, and each cell was run at temperatures up to 10,000 Kelvin. Simulation results were plotted, analyzed, and compared to those presented in the literature. Overall, results show pressure divergence that differs substantially with current DFT models of warm dense carbon. This work continues the application of MD simulations to WDM and provides a basis for future research into thermodynamic properties of warm dense plasmas.

Table of Contents

Introduction	4
Chapter 1: Warm Dense Carbon Plasmas	7
1.1 <i>Carbon Phase Diagram</i>	7
1.2 <i>Equations of State</i>	10
Chapter 2: Physics Models	14
2.1 <i>Density Functional Theory</i>	14
2.2 <i>Pseudopotentials & Planewaves</i>	18
2.3 <i>Car-Parrinello Molecular Dynamics</i>	20
Chapter 3: Quantum Espresso Code	22
3.1 <i>Introduction</i>	22
3.2 <i>Input Data</i>	25
3.3 <i>Post-Processing</i>	29
Chapter 4: Results	30
4.1 <i>Carbon Isochores</i>	30
4.2 <i>Discussion</i>	32
Conclusions	36
Author's Presentations: Conferences	38
References	39
Appendix	41
Vita	44

Introduction

Warm dense matter (WDM) describes the state of material that exists at high pressure and temperature regimes. Technically, WDM is matter that lies “between cold condensed matter and hot plasmas” (Redmer, Nettelmann, Holst, Kietzmann, & French, 2008). The density of WDM is on the order of traditional solids, but the temperature range extends to several thousand Kelvin (K). In this range, the amounts of an electron’s kinetic and potential energies are comparable due to partial ionization created by the extreme temperature, a phenomenon which results in a fluid-like plasma phase (Redmer, Nettelmann, Holst, Kietzmann, & French, 2008).

Interest in WDM largely derives from the field of astrophysics, where it is widely believed to compose the cores of giant planets and small stars in the universe. Further research into and subsequent enlarged comprehension of warm dense gases like hydrogen, helium, and carbon may uncover the secrets of the origin and inner workings of our universe. More practical is the process occurring within these stars, nuclear fusion. Thus an understanding of WDM is “of high importance” in learning the process of achieving conditions that facilitate nuclear fusion (Militzer, González-Cataldo, Zhang, Driver, & Soubiran, 2021). WDM is likewise expected to exist within Earth’s interior (Bonitz, et al., 2020). On Earth’s surface, however, it is much more elusive, as generation of WDM requires extreme amounts of energy and or very powerful radiation fields. Thus the need for such significant energetic quantities restricts the physical analysis and characterization of WDM, as only high-energy lasers, X-ray sources and nuclear blasts meet this substantial requirement (Bonitz, et al., 2020).

Therefore, man’s knowledge of WDM and its behavior must come from the formulation of theoretical models. Unfortunately, modelling WDM has several challenges. First, warm dense

systems are very diverse, characterized by “electronic quantum effects, moderate to strong Coulomb correlations, and finite temperature effects” (Bonitz, et al., 2020). In simpler terms, there are very complex interactions between electrons and nuclei *and* other electrons that occur in the warm dense region. Additionally, warm dense systems which are likely to be studied will themselves be very intricate – heterogeneous mixtures with large numbers of atoms. The resulting high densities and strong interactions render typical plasma theory models inapplicable (Militzer, González-Cataldo, Zhang, Driver, & Soubiran, 2021).

Fortunately, progress in various fields has improved the models of plasma states. Developments in quantum kinetic theory are an example (Bonitz, et al., 2020), but perhaps the greatest breakthrough was produced by the advent of density functional theory (DFT) and its growing role in molecular dynamics (MD) simulations. In applying the Kohn-Sham equations, DFT first allowed “self-consistent simulation of realistic warm dense matter [including] both plasma and condensed matter phases” (Bonitz, et al., 2020). However, at the high temperatures characteristic of WDM, DFT-MD simulations are “extremely challenging to perform” as there is a large number of diverse electron states to account for (Benedict, et al., 2014). Another issue arises from the unknown accuracy in DFT’s calculation of the exchange-correlation functional¹ (Bonitz, et al., 2020). Despite such obstacles, advances in DFT-MD simulations will continue to facilitate the production of accurate equations of state (EOS) which describe WDM.

Generally, the larger the size of the modelled system, the greater the required effort, computer time, and inherent difficulty in both forming and running a simulation. Therefore, pure systems comprised of low-atomic number elements are used as a simpler starting point and are a

¹In quantum mechanics, the exchange-correlation derives from two sources: i) Exchange interactions between indistinguishable, identical electrons and ii) correlation interactions due to the effect one electron’s motion has on another’s.

more practical basis of modeling WDM (Bonitz, et al., 2020). Carbon is particularly appropriate, as it is a well-studied and well-understood element that is abundant in the universe, on Earth, and in the human body. Both carbon's fit to the criteria described previously and its relative abundance of available experimental and simulation data make it an ideal candidate for exploring the warm dense phase.

This thesis utilizes the DFT-MD approach and the computer code Quantum ESPRESSO (QE) to model elemental carbon in the warm dense region. In the first two Chapters, an introduction to the carbon EOS and an overview of fundamental DFT-MD theory are provided. Chapter 3 provides a summary and construction of the particular QE code relevant to the project, the results of which are given in Chapter 4. In short, carbon cells of varying density are tested at temperatures between 0 and 10,000 K, and a discussion follows of how this thesis' results compare to those of previous works. Although carbon is the focus here, the overall goal of this thesis is to further the development of effective EOS and DFT models for warm dense plasmas.

Chapter 1: Warm Dense Carbon Plasmas

1.1 Carbon Phase Diagram

In practical, everyday settings, ambient temperature and pressure conditions manifest two phases of solid carbon: Diamond and graphite. Diamond, unsurprisingly, exhibits a diamond cubic crystal structure and is the hardest material known to man (Grumbach & Martin, 1996). Although creation of diamond requires large values of both temperature and pressure, it exists and is stable at lower pressure-temperature regimes (Grumbach & Martin, 1996). In contrast, graphite's hexagonal geometry is the preferred crystal structure under ambient conditions. Despite its weak inter-planar bonding, graphite sheets are the “strongest two-dimensional material known [to man]” (Grumbach & Martin, 1996). For the majority of humans' existence, these were the only carbon phases encountered in nature.

Technically known in science as carbon “allotropes,” both graphite and diamond possess remarkable properties which provide them a wide variety of practical uses (Pierson, 1993). Our ancient ancestors and schoolchildren alike know of graphite's ubiquitous function as pencil lead; in fact, the word

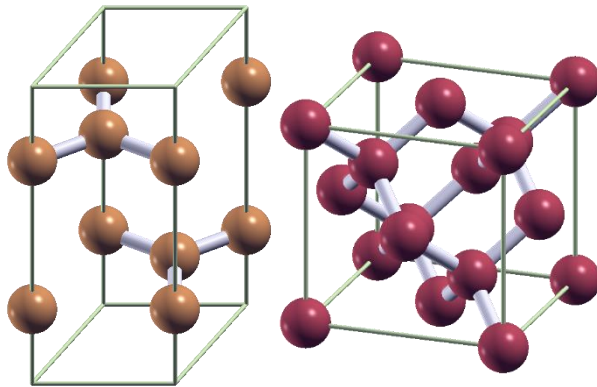


Figure 1-1. Reduced sphere depictions of diamond (right) and graphite unit cells. Reproduced from (Kokalj, 1999).

graphite actually stems from the Greek word meaning “to write” (Pierson, 1993). Both graphite's abundance and structure make it the building block of a “large variety” of complex materials such as those used in gas adsorption (typically called ‘activated’ carbon), “extremely strong” fibers, and lubricants (Pierson, 1993). Furthermore its strong ability to absorb neutrons facilitates graphite's

role as control rods in nuclear reactors. Beyond comprising the ideal wedding ring, diamond's use in industry is very diverse. In addition to its superior hardness, diamond also exhibits the greatest room-temperature thermal conductivity of any solid and is the model optical material for light transmission (Pierson, 1993). Diamond is scarce and thus very expensive and in high demand, three facts motivating its man-made synthesis (Pierson, 1993).

Given these reasons and considering the relative abundance of each allotrope, physically manufacturing the transition from graphite to diamond has long been a goal of science. However, the “dramatically different” bonding in their structures renders the transition very difficult to achieve at room temperature (Grumbach & Martin, 1996). When first accomplished in the 1950s, the graphite-diamond transition required the use of transition-metal catalysts (Grumbach & Martin, 1996). Furthermore, continuing to raise carbon's temperature and pressure beyond the diamond phase produces several other solid phases that are considered “diverse [and] unique among the elements” (Grumbach & Martin, 1996) However, phase boundaries and melting properties at these extreme conditions are “poorly known,” and experimental investigation of such transitions is limited, as the largest pressures humanly attainable are much lower than those observed in the transition (Correa, Bonev, & Galli, 2006). Regardless, based on DFT simulations, it is widely expected that carbon transitions from diamond to a solid with BC-8 symmetry at ~1,000 GPa and from this BC-8

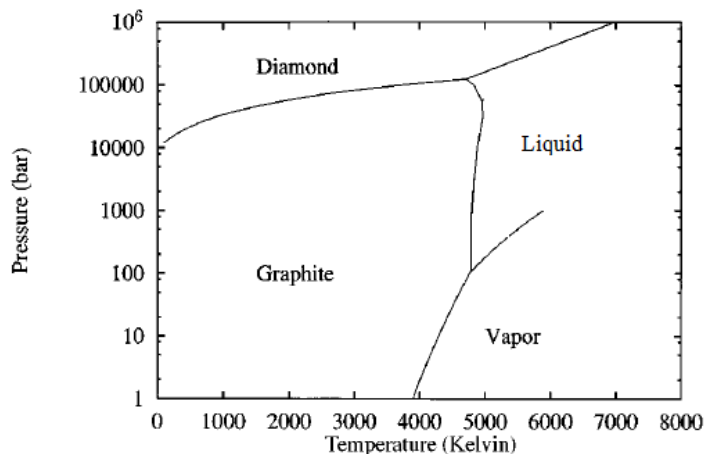


Figure 1-2. Proposed pressure-temperature phase diagram of carbon showing solid and liquid phases. Adapted from (Grumbach & Martin, 1996).

phase to a solid simple cubic (SC) phase at ~3,000 GPa (Correa, Bonev, & Galli, 2006; Martinez-Canales, Pickard, & Needs, 2012).

Interestingly enough, the slope of carbon's high-pressure phase boundary has actually sparked historical controversy between scientists. The dispute centered on whether carbon's behavior mimicked that of its same-period elements silicon and germanium – that is, whether its pressure decreased with a corresponding increase in melting temperature (Redmer, Nettelmann, Holst, Kietzmann, & French, 2008). This so-called melting slope is negative in both silicon and germanium. However, as later shown with DFT MD, an increase in the melting point of carbon produced an increase in the overall pressure and thus a positive melting slope (Parrinello, 1990). This behavior has interesting implications for the Earth's interior, as the positive slope of the melting line suggests that all free carbon existing within the Earth is in fact solid diamond and not liquid carbon (Grumbach & Martin, 1996). Similarly, this knowledge also improves our models of planetary and stellar bodies, as warm dense carbon is thought to comprise the majority of Uranus, Neptune, and white dwarf stars (Correa, Bonev, & Galli, 2006).

1.2 Equations of State

In molecular dynamics simulations, electrons and nuclei are considered separately, and nuclei are thus treated as distinct particles with corresponding positive charges. Therefore, the terms ‘nuclei’ and ‘ions’ are used interchangeably in DFT-MD and throughout this work. Forming EOS for WDM requires a few “basic” parameters termed “degeneracy parameters,” which exist for both electrons and ions. (Bonitz, et al., 2020). Electron degeneracy arises from the application of the Pauli Exclusion Principle, the inhibition of any two same-spin particles from occupying the same quantum state, to matter under intense pressure. As matter is compressed into smaller volumes of space, resulting electronic repulsions generates a pressure acting counter to the compression. Such pressure is termed degeneracy pressure and is thought to be what enables the existence of white dwarves, and other extremely dense bodies, by preventing total gravitational collapse (Akbari-Moghanjoughi, 2013).

Although degeneracy exists for both ions and electrons, ion degeneracy is “typically negligible” for WDM (Bonitz, et al., 2020). Electron degeneracy parameters are given below.

$$\theta = \frac{k_B T}{E_F} \quad (\text{Equation 1-1})$$

$$\chi = n\lambda^3 \quad (\text{Equation 1-2})$$

Above, θ and χ are degeneracy parameters, k_B the Boltzmann constant ($1.38 \cdot 10^{-23}$ joules per Kelvin – J/K), T temperature, E_F the Fermi energy, n the electron density, and λ the thermal de Broglie wavelength. Equation 1-1 gives the reduced temperature, which compares the statistical kinetic (thermal) energy of electrons to their Fermi energy – the difference in energy between the highest and lowest occupied single-particle states in a system of non-interacting electrons at zero temperature (Akbari-Moghanjoughi, 2013). The greater this ratio, the greater the electron

degeneracy. Equation 1-2 relates the electron density and their de Broglie wavelength; it is effectively a measure of the number of electrons within the system (Akbari-Moghanjoughi, 2013). Similar to the first parameter, the higher the number of electrons in a given amount of space, the greater the resulting degeneracy pressure.

Additionally, two parameters are used to account for classical and quantum coupling between nuclei and electrons, respectively (Bonitz, et al., 2020). Accounting for ion-ion interactions, the ionic coupling parameter is the ratio of ionic potential and kinetic energies:

$$\Gamma_I = \frac{Q_I^2}{a_I k_B T} \quad (\text{Equation 1-3})$$

where the variable Γ_I represents the coupling parameter, Q_I the ionic charge, and a_I the mean inter-ionic distance. The squared charge assumes a homogeneous system of ions. Electron coupling is given by Equation 1-4.

$$r_s = \frac{a}{a_B} \quad (\text{Equation 1-4})$$

Above, r_s is the electron coupling parameter, a the average distance between electrons, and a_B the Bohr radius – the most probable distance between the proton and electron in a ground state hydrogen atom $-5.29 \cdot 10^{-11}$ meters (Akbari-Moghanjoughi, 2013). Known as the Wigner-Seitz (WS) radius, the value of r_s is the radius of a sphere whose volume is equal to the mean volume per free electron in condensed matter systems (Bonitz, et al., 2020) and as such is effectively a measure of the electron density of the system. The lower the WS radius, the greater the electron coupling. Both degeneracy and coupling parameters are combined with traditional EOS variables – specific volume, atomic radii, and the like – to form EOS for complex systems like WDM.

Since DFT first allowed the simulation of warm dense plasmas, a variety of technical methods employing DFT have been, and continue to be, utilized to improve the carbon phase diagram and its corresponding EOS. In 2012, Martinez-Canales, et al. used the DFT code

CASTEP to model carbon cells at extreme pressures by relaxing “randomly chosen structures” to their minimum in enthalpy. Their results support both the existence of the BC-8 and SC phases and their proposed transition pressures (Martinez-Canales, Pickard, & Needs, 2012). Despite a lack of “direct experimental evidence” for such stability at high pressures, they note that, because of trends observed in similar metals, the existence of multiple phase transitions in solid carbon is likely. In fact, their simulations also support the existence of at least four more solid phases: (i) a simple hexagonal (SH) transition at ~6,000 GPa, (ii) face-centered cubic (FCC) at ~21,000 GPa, (iii) double hexagonal close packed (DHCP) at ~270,000 GPa, and (iv) body-centered cubic (BCC) at ~640,000 GPa (Martinez-Canales, Pickard, & Needs, 2012).

Beyond the solid phases, both liquid and vapor phases of carbon exist, albeit at extreme combinations of temperature and pressure. Furthermore, DFT simulations support the existence of *multiple* distinct liquid phases as well as several corresponding triple points between solid, liquid and or vapor phases (Grumbach & Martin, 1996). Formation of an applicable EOS for liquid carbon occurs entirely via the application of theory to computer simulations. Benedict, et al. fitted available data from DFT MD and path integral Monte Carlo (PIMC) simulations to present an EOS for four solid phases of carbon (diamond, BC-8, SC, SH) and the liquid phase. Their EOS uses 24 variables to readily “account for the effects of ionization due to temperature and pressure in the plasma state” (Benedict, et al., 2014). However, their study notes a limit in the application of DFT methods posed by its lower accuracy at very high temperatures (Benedict, et al., 2014).

Most exchange-correlation potentials utilized in DFT calculations were first proposed by Perdew and Wang (the PW functional) and Perdew, Burke, and Ernzerhof (PBE). However, these calculations, and their corresponding potentials, assume zero temperature, an assumption which provokes opposition to their utilization in finite- (non-zero) temperature simulations (Bonitz, et

al., 2020). Recently, Bonitz, et al. modeled warm dense carbon using both PW and PBE functionals, DFT MD, and Quantum-ESPRESSO code. They compared their results to those generated using a finite-temperature functional (Bonitz, et al., 2020). In their conclusions, they note relatively small deviation between the zero- and finite-temperature functionals (Bonitz, et al., 2020). Although it is possible that, as the temperature is increased further, the specific exchange-correlation potential chosen may become insignificant, as the closer the system's temperature to the classical plasma regime, the less prominent the many-body effects that cause such deviation (Bonitz, et al., 2020). Nevertheless, improvements in DFT, its assumptions, and core calculations represent both the initial breakthrough that made possible simulations of WDM *and* the current obstacles preventing the generation of consistent and reliable WDM EOS.

Chapter 2: Physics Models

2.1 *Density Functional Theory*

The history of DFT coincides with the growth of both interest in and knowledge of the atom and interatomic forces. In particular, both the “discovery” of quantum mechanics in the early 1900s and the advent of atomic and molecular orbital theories in the second half of the 20th century facilitated greater understanding of the atom, atomic bonding and, eventually, the development of DFT (Haunschild, Barth, & French, 2019). However, it was not until the 1960s that the “foundational publications for modern DFT” were established (Haunschild, Barth, & French, 2019). Two publications, Hohenberg and Kohn (1964) and Kohn and Sham (1965), laid the groundwork of modern DFT by applying the Hartree-Fock method of determining electronic wavefunctions to molecules and solids (Haunschild, Barth, & French, 2019).

Since then, DFT has grown in complexity and application. Building on DFT’s foundation, modern works have produced improvements in self-consistency calculations, increased understanding of atomic and molecular orbitals, created iterative methods of simulating molecular dynamics, included time-dependent variables in DFT calculations, and, ultimately, used DFT in a smorgasbord of different applications (Haunschild, Barth, & French, 2019). Examples of this variety include the bonding within halogen systems (Ang, Ser, & Wong, 2019) and limiting corrosion in electrochemical systems (Obot, Macdonald, & Gasem, 2015). However, DFT remains a work in progress as improvements to its accuracy and capabilities are continually ongoing. As such, alternative methodologies stemming from traditional DFT that apply similar principles to model atomic systems have arisen as well. One such methodology, subsystem DFT, changes the typical representation of and subsequent calculation of the ground state electron density (Jacob & Neugebauer, 2014). Simply summarized, DFT is a computational method which blends physics,

mathematics, and computer science to analyze the structure of atoms, molecules and crystals and the interactions within them.

Condensed matter physics and materials science predict material properties through an understanding of systems' interacting electrons and atomic nuclei (Singh, 1994). Schrodinger's equation (Equation 2-1) is the quantum representation of classical energy conservation – at atomic and molecular scales, interatomic potential forces are non-negligible, and thus the kinetic energy alone is insufficient in defining a system.

$$H_{op}\Psi(r,t)=E\Psi(r,t)=(K+\Phi)\Psi(r,t) \quad (\text{Equation 2-1})$$

Here H_{op} is the Hamiltonian operator, E the total energy of the electron, K and Φ the electron's kinetic and potential energies, respectively, and Ψ the (electron) wavefunction, which itself is a function of both its position, r , and time, t . Qualitatively, H_{op} (the sum of kinetic and potential energy) is performed on a given electron, or wavefunction, to determine its total energy. Electronic configurations that minimize the energy are the most stable.

The majority of materials, however, have systems with multiple, discrete levels of many electrons that constantly interact. Modelling such systems via a solution to Schrodinger's equation is extremely difficult and instead requires “sufficiently accurate, but tractable [and] approximate techniques,” (Singh, 1994). DFT is an example of such a technique. The primary theorem upon which DFT is based is the first Hohenberg-Kohn theorem, which states that the total energy, E , of a system of interacting electrons is purely a function of the ground state electron density, ρ (Obot, Macdonald, & Gasem, 2015).

$$E=E(\rho) \quad (\text{Equation 2-2})$$

The “true” ground state density is the one that minimizes the total energy of the system, and other ground state properties are likewise functions (called ‘functionals’) of this true ground

state (Singh, 1994). Thus the origin of the term ‘density functional theory.’ Finding the ground state density is typically done through iteration. These ‘self-consistent,’ or Hartree-Fock, calculations iterate through different arrangements of atoms and electrons until a desired level of convergence is achieved. In practice, reaching the ground state energy is difficult. It was first modeled as the sum of the total Hartree (or Coulomb) energy and an unknown, smaller density functional called the “exchange-correlation functional” (Singh, 1994). This sum is given in Equation 2-3.

$$E(\rho)=K_S(\rho)+E_{ei}(\rho)+E_{ii}(\rho)+E_H(\rho)+E_{xc}(\rho) \quad (\text{Equation 2-3})$$

The total of the particle’s kinetic energy is given by K_S , Coulombic interactions between electrons and nuclei by E_{ei} , repulsive interactions between nuclei by E_{ii} , interactions between electrons by E_H , and the unknown exchange-correlation (xc) energy by E_{xc} .

Actually predating DFT is the local-density approximation (LDA). First developed by Slater in 1951, the LDA’s use in solid state physics was initially “limited” before becoming more commonplace in the 1970s (Singh, 1994). Considered the “simplest form of DFT,” the LDA first declared the exchange-correlation energy a functional of electron density (Obot, Macdonald, & Gasem, 2015). The approximation is given in Equation 2-4, where the variable ϵ_{xc} is the exchange-correlation energy per particle.

$$E_{xc}^{LDA}(\rho)=\int \rho(r)\epsilon_{xc}(\rho)dr \quad (\text{Equation 2-4})$$

However, in 1965, Kohn and Sham modified this approach, instead deriving the electron density as a “self-consistent solution of a set of single particle Schrodinger-like equations” (Singh, 1994). Known as the Kohn-Sham (KS) equations, these density-dependent single particle equations utilize individual particle orbitals and potentials (Singh, 1994).

$$[K+V_{ei}(r)+V_H(r)+V_{xc}(r)]\phi_i(r)=\epsilon_i\phi_i(r) \quad (\text{Equation 2-5})$$

In Equation 2-5 above, K is the particle's kinetic energy, V_{ei} the Coulomb potential between the particle and any nuclei, V_H the Hartree potential due to electron-electron interactions, V_{xc} the exchange-correlation potential, φ_i the orbital of particle i , and ϵ_i their corresponding eigenvalues. The electron density is estimated and used to predict the value of V_{xc} , the only unknown in Equation 2-4 (Singh, 1994). This value is then in turn used to predict the unknown exchange-correlation energy via Equation 2-6 (Parrinello, 1990).

$$V_{xc}(\mathbf{r}) = \frac{\delta E_{xc}(\rho)}{\delta \rho(\mathbf{r})} \quad (\text{Equation 2-6})$$

Next, the value of E_{xc} is inserted into the original set of single particle equations (Equation 2-5) and the resulting electron density, ρ , is determined. The value of ρ *must* reproduce the initial estimate of the electron density within a desired level of convergence (Singh, 1994). This iterative process describes the self-consistent nature of the Kohn-Sham method.

An understanding of other, more complex features of DFT, such as fast Fourier transforms and the differences between spin-polarized and non-spin systems, was not required in this work. Rather, the above simplification of DFT enabled a basic knowledge of DFT and its central theory that proved helpful in understanding, visualizing, and altering Quantum ESPRESSO input and output.

2.2 Pseudopotentials & Planewaves

As mentioned previously, matter is made of complex, many-electron systems that interact strongly with atomic nuclei via Coulombic potential forces. Electrons are classified as either ‘core’ (inner orbital) or ‘valence’ (those lying in the outermost orbital). In most cases, core electrons are strongly bound by the positively-charged nucleus and do not respond to the motion of valence electrons; thus they are considered essentially fixed (Singh, 1994). This is known as the ‘frozen core’ approximation, which is generally reliable and lies at the heart of pseudopotential methods.

Therefore the complex effect of core electron motion and the nucleus on valence electrons is replaced with an effective potential, called a pseudopotential. Similarly, the valence electron wavefunctions are expanded using a set of basis functions to account for the pseudopotential and are correspondingly called pseudo-wavefunctions. In general, such basis sets are quantitative representations of atomic and molecular orbitals. Quantum ESPRESSO code utilizes planewave basis sets (Giannozzi, et al., 2009), which represent orbital wavefunctions by linear combinations of expanded Fourier series (Stuart & Mosey, 2020).

Construction of pseudopotentials is done so in as practical a manner as possible. They are often required to be both “soft” and “transferable” (Singh, 1994). A soft pseudopotential allows “expansion of the valence pseudo-wavefunctions

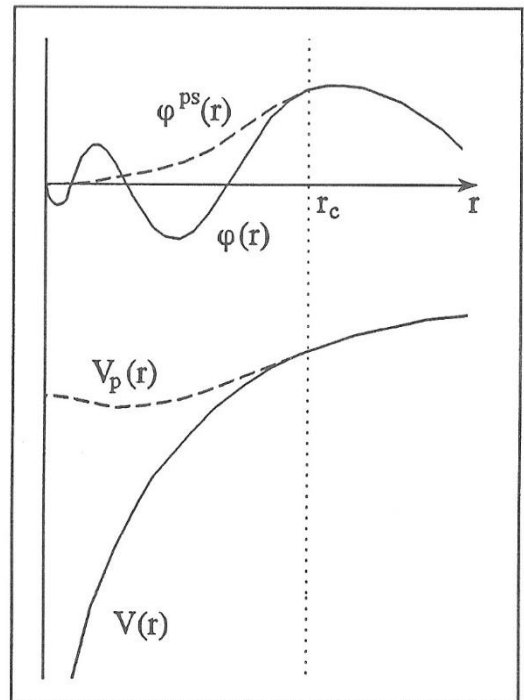


Figure 1-1. Illustration of how the all-electron wave function, $V(r)$, and core potential, $\phi(r)$, are replaced by the pseudo-wavefunction, $V_p(r)$, and the pseudopotential, $\phi^{ps}(r)$. Here, r_c is the core (or “cut-off”) radius.

Adapted from (Singh, 1994).

using as few planewaves as possible” (Singh, 1994). However, for first-row elements, like carbon, a large number of planewaves is needed to effectively “describe ‘localized’ 2p valence states” (Kresse & Hafner, 1994). Additionally, a pseudopotential is said to be transferable if, when generated for a given atomic configuration, it accurately reproduces other configurations (Singh, 1994). Such a pseudopotential is considered reliable in solid state applications. Finally, a pseudopotential should produce an electron “pseudo-charge density” that accurately mimics the actual charge density (Singh, 1994).

The principle of ‘norm-conservation’ (NC) helped make possible meeting these dual requirements of softness and transferability (Singh, 1994). The NC constraint requires that, while outside the core radius, pseudo-wavefunctions (and potential) are equal to the actual valence wavefunctions, within the core radius, the pseudo-wavefunctions may differ from the true wavefunctions so long as the overall enclosed charge (the ‘norm’) is the same (Kresse & Hafner, 1994). This constraint provides for consistent transferable pseudopotentials (Singh, 1994) which are frequently employed in MD simulations.

Due to the requirements of the Car-Parrinello package in Quantum ESPRESSO, only ultrasoft (US) pseudopotentials are utilized in this work. First proposed by Vanderbilt in 1990 for utilization in large-scale simulations, US pseudopotentials and accompanying pseudo-wavefunctions within the core are made soft by “relaxing the norm-conservation constraint” (Kresse & Hafner, 1994). While removing the NC requirement complicates calculations by allowing the pseudopotential itself to change during the calculation, the accuracy of the calculation itself is not sacrificed (Singh, 1994). The primary benefits of US pseudopotentials are their reduction in the minimum energy cutoff of the planewave basis set and a corresponding decrease in the overall “cost” of the calculation (Singh, 1994).

2.3 Car-Parrinello Molecular Dynamics

The theory behind Car-Parrinello MD (CPMD) is similar to that of Born-Oppenheimer MD (BOMD), although they differ in calculation of the electron ground state density. First consider the Born-Oppenheimer (BO) potential energy surface, Φ , of a multiatomic system. MD models of the BO system follow Newton's equation of motion below.

$$M_I \ddot{R}_I = -\frac{\partial \Phi}{\partial R_I} \quad (\text{Equation 2-7})$$

The variables M_I and R_I represent, respectively, the mass of nucleus I and the corresponding ionic positions (Car & Parrinello, 1985). Additionally, a dot above a variable ($\dot{\quad}$) denotes its time derivative, so the variable \ddot{R}_I represents the second time derivative of an ion's position (its acceleration).

The Born-Oppenheimer method solves Equation 2-7 for a given ionic configuration *and* performs a full electronic structure calculation at every time step (Redmer, Nettelmann, Holst, Kietzmann, & French, 2008). In real systems, this procedure produces reliable physical dynamics but, unfortunately, it is also considered “computationally very demanding” (Car & Parrinello, 1985). Instead, Car-Parrinello calculations assume a “fictitious” dynamical system that removes this expensive requirement (Car & Parrinello, 1985). Doing so provides a more efficient and convenient method of achieving self-consistency and modeling atomic motion and the resulting forces. CPMD treats the energy functional, $E(\rho)$, as “the potential energy surface of a fictitious classical dynamic system consisting of the nuclear plus the electronic degrees of freedom” (Parrinello, 1990). The corresponding equations of motion are shown on the next page.

$$M_I \ddot{R}_I = - \frac{\partial E}{\partial R_I(t)} \quad (\text{Equation 2-8})$$

$$\mu \ddot{\phi}_i(r,t) = - \frac{1}{2} \frac{\delta E}{\delta \phi_i^*(r,t)} + \sum_j \Lambda_{ij} \phi_j(r,t) \quad (\text{Equation 2-9})$$

The ionic configurations, R_I , and the electron orbitals, ϕ_i , represent the aforementioned degrees of freedom.

The variable μ is an adjustable parameter considered the fictitious electron mass, and Λ_{ij} are Lagrangian multipliers inserted to preserve the orthonormality of the KS electron orbitals (Singh, 1994). The motion predicted by Equations 2-7 and 2-8 will differ. In other words, the surface produced in CPMD will deviate from the Born-Oppenheimer surface. To account for this, the value of μ is carefully selected to ensure that electron dynamics are “sufficiently faster” than those of the ions (Parrinello, 1990). An appropriate value of μ , therefore, provides a “negligible” error in the modeled forces (Kühne, 2014) and thus yields a surface “sufficiently close” to that of the BO method (Singh, 1994). Generally, the higher the value of μ , the more efficient and quicker the calculation. However, the deviation from the BO surface likewise increases (Singh, 1994), so a compromise must be made between accuracy and computational cost.

An additional parameter that affects the calculation’s efficiency is the time step, δt , at which each iteration of the simulation is executed. Increasing the time step will affect system dynamics in the same way as decreasing the value of μ . Given this inverse relationship, “judicious choices” of both δt and μ are required in CPMD simulations (Singh, 1994). Large values of μ (small δt) require a very large number of steps while a small μ (long δt) can produce an unstable solution (Singh, 1994). Similar disadvantages are faced when applying CPMD to systems of nonzero temperature as “thermal equilibration requires a very long time” (Parrinello, 1990).

Chapter 3: Quantum Espresso Code

3.1 Introduction

The suite of computer code that comprises Quantum ESPRESSO is based on DFT, planewaves, and pseudopotentials. In other words, QE seeks to build “chemically realistic” models of materials that are based on DFT by using a “plane waves basis set and pseudopotentials to represent electron-ion interactions,” (Giannozzi, et al., 2009). The name itself is an acronym which stands for: **opEn Source Package for Research in Electronic Structure, Simulation, and Optimization** (Giannozzi, et al., 2009). The software is free and available to researchers throughout the world. Despite containing a variety of packages and possessing widespread capabilities in MD calculations, this work makes use of only two: *PWscf* and *CP*.

3.1.1 PWscf

The package *PWscf* is used for self-consistency calculations. It can accommodate both norm-conserving and ultrasoft pseudopotentials in a variety of applications (Giannozzi, et al., 2009). In this work, however, the *PWscf* package is used only to produce figures of the ground state configuration of the input carbon cells. This was done with XCrySDen, a program built to visualize crystal structures (Kokalj, 1999). When used with QE, the XCrySDen program is compatible only with *PWscf* input and output.

3.1.2 CP

The *CP* package performs Car-Parrinello *ab initio* MD. As described earlier, *ab initio* dynamics allow for detailed calculations of atomic motion and interatomic forces without the expensive self-consistent minimization at every time step (Parrinello, 1990). *CP* performs simulations of both the NVE and NVT ensembles (Giannozzi, et al., 2009). The NVE, or microcanonical, ensemble performs calculations for which the number of atoms within, volume of, and total energy of the system are constant. The variables traditionally assigned to these parameters are N, V, and E, respectively. Similarly, the NVT, or canonical, ensemble allows for calculations at constant temperature, T, while energy is allowed to fluctuate. Simulations of both ensembles were utilized in this work.

Ultrasoft pseudopotentials are the only type used in the *CP* package. The QE program provides pseudopotentials for a variety of elements, including carbon – only one of which is utilized in this work. Shown results are for only the QE pseudopotential ‘C.pbe.rkkjus’ which makes use of the PBE generalized gradient approximation (GGA)¹.

Running a CPMD simulation in QE consists of four primary steps. Each step was formed and carried out via the guidelines outlined in the “CP User’s Guide” for Quantum ESPRESSO provided by Giannozzi, et al. Sample input files for select steps are provided in the Appendix. The steps are summarized on the following page.

- Apply Gram-Schmidt process: The system is first defined using the various input parameters in the *CP* package. Due to complex dynamics of electron wavefunctions within

¹ In DFT, the GGA is a density functional used to estimate the exchange-correlation potential, V_{xc} . It assumes the value of V_{xc} depends upon both the electron density, ρ , and its gradient, $\nabla\rho$. The GGA differs from the local density approximation (LDA), which assumes the electron density is uniform (zero gradient). Both approximations entail complex mathematics which require the use of computers. (Singh, 1994)

the 24-atom model, a brief (~50 time step) stage applies Gram-Schmidt orthonormalization to help the wavefunctions converge.

- Reach the electronic ground state: The system then reaches its electronic ground state. This is accomplished by applying steepest descent or damped dynamics to the electrons.
- Relax the system: Next, the nuclei, referred to as “ions,” are relaxed. This is done by minimizing the forces on each ion using steepest descent, damping, or both until an equilibrium is reached.
- Randomize ion positions: Before molecular dynamics can be run, the ions are moved slightly from their equilibrium positions. If not, no dynamics will occur, as the ions, and subsequently the system, are at equilibrium.
- Run CPMD NVE Ensemble: Prior to setting the temperature, the system is allowed to move via the Verlet algorithm under the constant energy NVE ensemble. This step is carried out long enough to show convergence in system pressure.
- Set the temperature and run CPMD: The desired temperature is then ‘controlled’ by rescaling of ionic velocities. This step is run long enough for the system to ‘thermalize’ at the given temperature. Due to inherent coupling in the system, many steps are required to achieve thermal equilibration, especially at greater temperatures. Similarly, the run will not end when a desired level of convergence is reached; rather the system will oscillate around the set temperature. Similar to the previous step, the dynamics occur via the Verlet algorithm.

3.2 *Input Data*

Carbon unit cells were comprised of 24 atoms assigned arbitrary positions (via a random number generator). The density of the cell is manipulated in one of two ways: either the number of carbon atoms in the unit cell or the size of the cell lattice parameter was altered. For consistency, only the lattice parameter was changed in this work. Simulations were run at densities 1, 2.26, and 10 grams per cubic centimeter (g/cm^3), values which correspond to lattice parameters of 8.1, 7.4, and 6.9 Bohr, respectively. Images of each unit cell, produced with the software XCrySDen, are shown below in **Figure 3-1**. Included in the Appendix are hard-sphere depictions and descriptions of each unit cell.

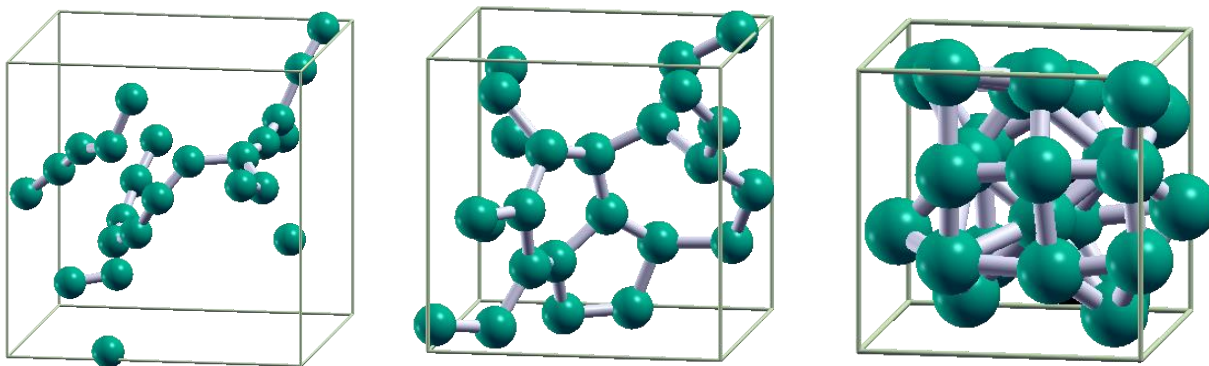


Figure 3-1. Reduced sphere unit cell depictions of carbon systems modeled in QE. Shown are densities 1 (left), 2.26 (center), and $10 \text{ g}/\text{cm}^3$. Reproduced from (Kokalj, 1999).

Although an arbitrary QE input file has several subsections, called “namelists,” and subfields, “cards,” only those with parameters relevant to the work are discussed here. Input files consist of the following namelists: Control, System, Electrons, and Ions. The Control namelist is used to define important convergence thresholds, the specific calculation being performed, and other logistical variables. The structure of the unit cell is defined in the System namelist. Desired dynamics for the electrons and nuclei are chosen in the Electrons and Ions namelists, respectively.

The number, type, and position of atoms in the simulation are also defined in the Atomic Species and Atomic Positions cards. (Giannozzi, et al., 2009)

Each step in a CP simulation runs the same calculation (“cp”), however each employs a different combination of variables to accomplish its goal. Those especially relevant to each specific step are as follows:

Gram-Schmidt	ortho	To apply Gram-Schmidt orthonormalization, the value is set to “Gram-Schmidt.” Running a brief stage with these dynamics is sometimes necessary to facilitate convergence of electron wavefunctions.
Electron relaxation ¹	restart_mode	Initially, the value is set to “from_scratch” to denote the beginning of a new trial. ²
	ndr, ndw	The specific values of these variables are arbitrary and default to “50, 50.” They are the memory slots from which input is read (ndr) and output is written (ndw). While arbitrary, their sequence relative to succeeding runs is important. ³
	dt	Due to the large system, 24 atoms, given random positions, a relatively small time step is required to run the simulation. Given in picoseconds, time steps of “2.5d0” and “5.0d0” are used in this work.
	celldm(1)	This variable is the lattice parameter of the unit cell, aforementioned in this chapter.
	ecutwfc	The kinetic energy cutoff value for the electron wave function, ecutwfc, is determined within the suggested range of the pseudopotential used.
	ecutrho	Due to the use of ultrasoft pseudopotentials, the value of the kinetic energy cutoff for charge density and potential is set to 8-12 times that of ecutwfc. In this work, 12 was used.

¹ An input file for a sample electron relaxation step is included in the Appendix. For clarity, all variables relevant to this work are included.

² If Gram-Schmidt (GS) is applied beforehand, then the value is “restart.”

³ Similarly, given GS is run initially, the value of “ndr” for the electron relaxation is equal to “ndw” of the GS step.

Electron relaxation (continued...)	electron_dynamics	Steepest descent dynamics are applied to reach the electronic ground state. This variable is set to “sd” and unchanged until molecular dynamics are run.
Cell (ion) relaxation	restart_mode	Because this step is a carry-over from the first, its restart mode is set to “restart,” meaning it reads its input from the output of the previous step.
	ndr, ndw	For the same reasons above, this step reads from the written slot of the electron relaxation and must write to a different slot. For example, if “50, 50” is used in the electron relaxation, “50, 51” is used in the cell relaxation. This trend continues in each successive step.
	ion_dynamics	Nuclei are required to reach their equilibrium positions. This is done by applying steepest descent (“sd”) or damped (“damp”) dynamics to the ions.
	atomic mass	The atomic masses used in the cell relaxation are lowered. This does not affect the accuracy of the calculation but rather is used to accelerate it. For example, the carbon atomic mass, 12.01 in all other steps, is lowered to 1.201 or 0.1201 to speed up ionic relaxation.
Random displacement of ions	ion_dynamics	After the cell is relaxed, dynamics are returned to “none.”
	tranp()	To dictate that the ions be displaced, this variable is set to “.TRUE.” The specific amplitude of the displacement is set using the variable amprp().
NVE ensemble	electron_dynamics	CP molecular dynamics is run by setting this variable to “verlet.”
	electron_velocities	At the start of a new molecular dynamics run, electron velocities are set to “zero.”
	ion_dynamics	Same as above, “verlet.”
	ion_velocities	Same as above, “zero.”
NVT ensemble	ion_temperature	The temperature is set by rescaling ionic velocities, so a value of “rescaling” is assigned to this variable.

NVT ensemble
(continued...)

tolp

The tolerance of velocity rescaling is measured in Kelvin. When ionic temperatures differ from the value of “tempw” by more than the value of “tolp,” rescaling is applied. The default value of 100 K was used.

tempw

The temperature of the system, in Kelvin. Important to note: The term *average* implies that the temperature of the system oscillates about this assigned value while the overall average measured will equal that of tempw.

3.3 *Post-Processing*

Equation of state parameters are set by defining the input mass, volume, and temperature and, the resulting system pressure is in turn calculated. A single CP run produces a variety of output .txt files that display given variables at every time step of the simulation. Such files provide a wealth of information, including atomic positions (.pos), atomic forces (.for), energies (.evp), and relevant Nosé-Hoover variables (.nos). The energies output file gives the potential, kinetic, and total energies of the system as well as the temperature of and pressure within the system. Results were quickly plotted with the helpful software package *gnuplot*, although more detailed charts were produced using Microsoft Excel. Examples of which are given in Chapter 4.

Chapter 4: Results

4.1 Carbon Isochores

Each carbon isochore was simulated at temperatures up to 10,000 K, although the 10 g/cm³ cell was also modeled up to 20,000 K. **Figures 4-1** and **4-2** show plots of cell temperature and pressure versus simulation time – given in picoseconds (ps) (1 ps = 10⁻¹² s) – of the 10 g/cm³ cell modeled at 10,000 K. The applied temperature is instantaneously reached, and oscillations about it (controlled via the value of parameter “tolp”) are clearly observed in the plots. In contrast, the pressure increases drastically before slowing its increase and not completely converging. As with the temperature, pressure oscillations are also present and easily observed. Each trial was executed in the following manner: following the microcanonical NVE stage (conducted at 0 K), the desired temperature was applied and the system allowed approximately 50 picoseconds to equilibrate.

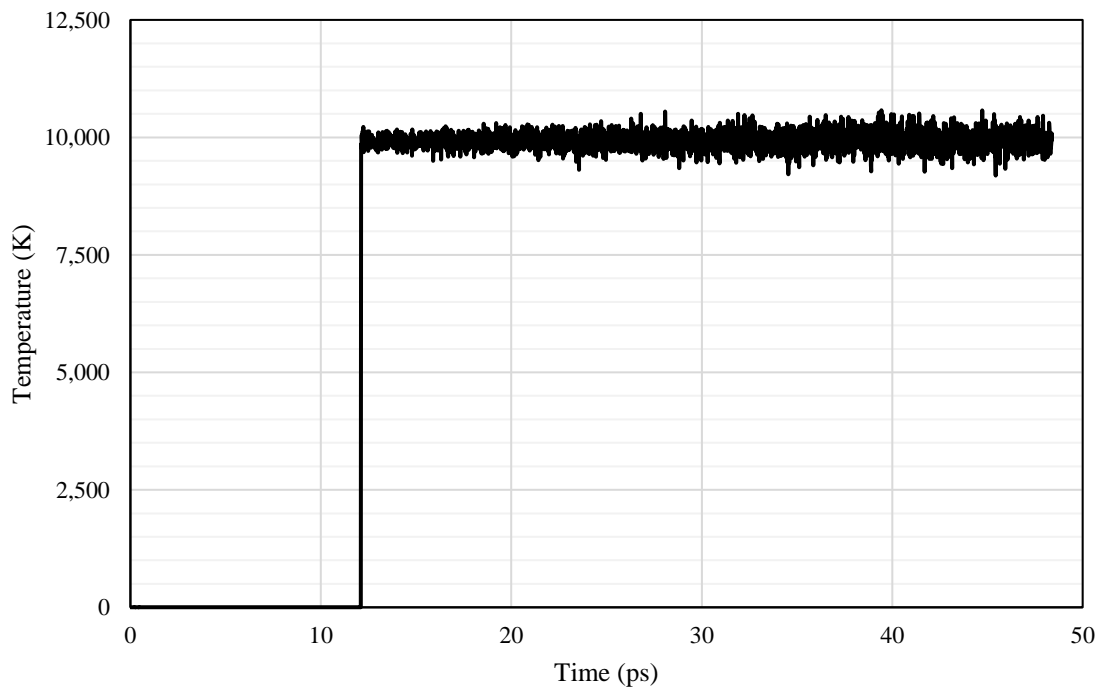


Figure 4-1. Temperature versus time for carbon cell of density 10 g/cm³ modeled at 10,000 K. Produced using QE CPMD output .evp files and Microsoft Excel.

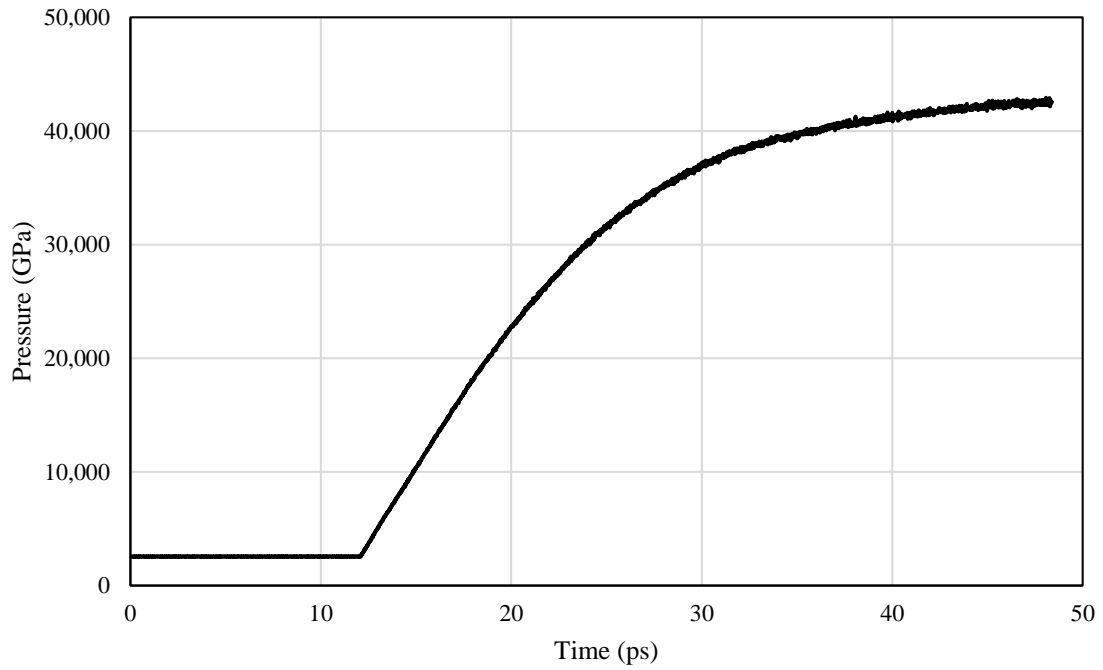


Figure 4-2. Pressure versus time for carbon cell of density 10 g/cm^3 at $10,000 \text{ K}$.

Similar results were observed across all simulated temperatures and for both 1 and 2.26 g/cm^3 isochores.

4.2 Discussion

Because the pressure continues to rise (diverge), reliable estimates cannot be made. Thus estimations of system pressure are not provided in this work. However, the results of this work may still be compared to those encountered in the literature¹, from which they substantially differ. For example, in their work, Bonitz, et al. presented quantum MD results for a carbon cell of density 10 g/cm³. Their 32-atom system employed a projector augmented-wave (PAW) pseudopotential and the Andersen thermostat in the *PWscf* package of QE. At 10,000 K, Bonitz, et al. predicts a pressure of ~1,700 GPa, while this work shows pressures increasing beyond 33,000 GPa, differing by a factor of about 20. This deviation factor increases with temperature and is consistent for all of the isochores simulated in this work. Furthermore, results similar to those of Bonitz, et al. were produced by Militzer, et al. and Benedict, et al., both of which utilized the Vienna Ab initio Simulation Package (VASP) code and PAW pseudopotentials to model their systems.

There are several procedural differences between this work and those of the literature, but it is difficult to ascertain the exact cause of the stark difference in pressure behavior. While the numbers of atoms in each unit cell are not the same across each work, it is unlikely that this variable would create such different results, as the systems used various numbers of atoms (32 in Bonitz, et al. and 64 in Benedict, et al.) but generated similar data. Additionally, results in literature are produced using various DFT-MD codes, with consistent EOS data produced in both VASP and QE. Perhaps the deviation arises from the type of MD executed. Bonitz, et al. follows the method outlined by Zhang, et al. which applies Born-Oppenheimer MD to systems at WDM-like temperatures. The deviation of Car-Parrinello MD from the BO method is discussed in Chapter

¹ MD simulation results from this work are compared to warm dense carbon EOS data given by Militzer, et al. (2021), Bonitz, et al (2020), and Benedict, et al. (2014).

2, and it is possible that the fictitious parameters used by CPMD in this work produce results that so significantly differ from those by traditional BOMD. However, the VASP code utilizes *ab initio* MD, which are similar to those in the *CP* package of QE, and yields consistent data.

Furthermore, Bonitz, et al. sets the temperature by applying the Andersen thermostat, which is not an option for temperature control in the *CP* package. Although CPMD in QE offers application of the Nosé-Hoover (NH) thermostat, rescaling of ion velocities was employed as the chief means of temperature control in this work. Preliminary simulations utilizing the NH thermostat showed smooth thermal equilibration at temperatures below 500 K but severe fluctuations (up to ± 25 percent of the target temperature) at higher temperatures. In contrast, velocity rescaling works by applying some factor to all particle velocities. Dubbed the “rescaling factor,” it is calculated by forcing the total kinetic energy to equal the average kinetic energy of the system at the target temperature (Bussi, Donadio, & Parrinello, 2007). **Figure 4-4** depicts two simulations of carbon at 10 g/cm^3 and 20,000 K, one which applied the NH thermostat, and the other velocity rescaling. **Figure 4-5** shows the corresponding pressures of both systems.

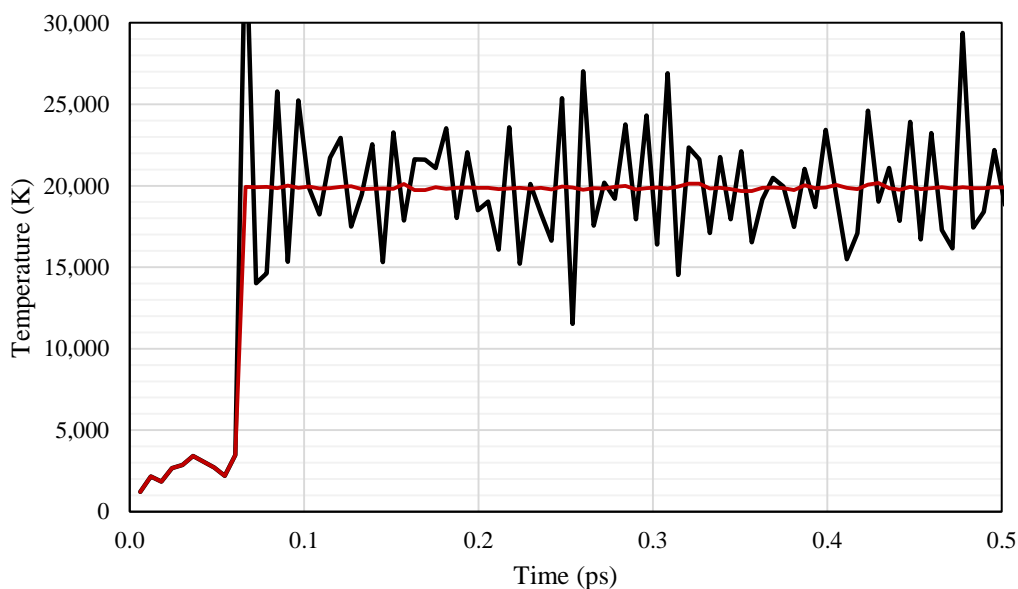


Figure 4-4. Temperature of 10 g/cm^3 isochore simulated at 20,000 K controlled via velocity rescaling (red) and the Nosé-Hoover thermostat. The simulation, actually carried out for ~ 50 ps, is magnified to better show the fluctuation.

As is observed, despite the much different temperature fluctuation between the two methods, both velocity rescaling and the NH thermostat produce comparable results. The figure shows only the initial 0.5 ps of the simulation, but the trends in both temperature and pressure are consistent throughout its entirety. Therefore, given this and for other, aforementioned reasons, it is more probable that the discrepancy between this work and the accepted literature arises from either the setup of the carbon unit cell and or the procedure used in each simulation. As already

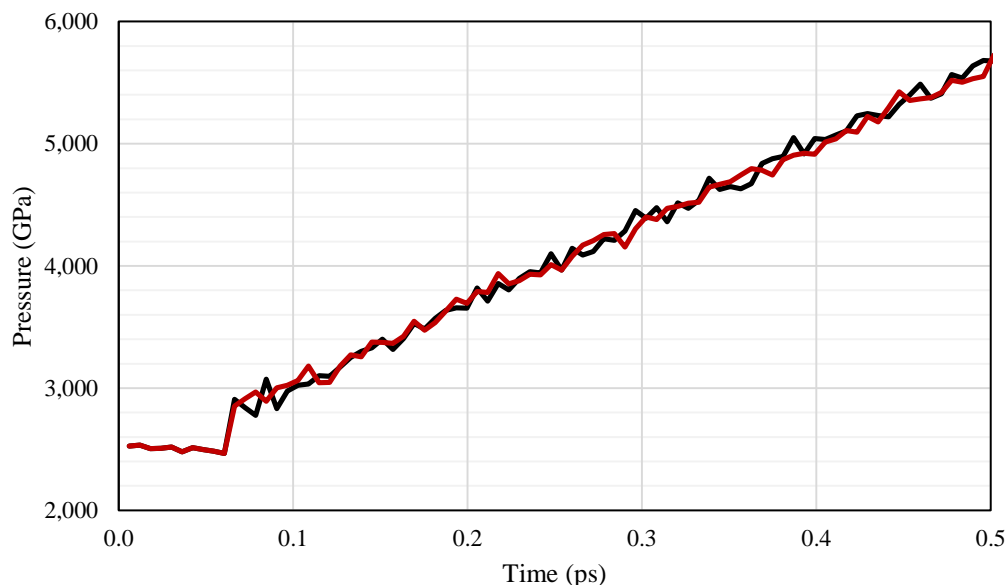


Figure 4-4. Temperature of 10 g/cm³ isochole simulated at 20,000 K, controlled via velocity rescaling (red) and the Nosé-Hoover thermostat.

noted, the number of atoms chosen in this work, 24, is lower than that of any of the carbon cells encountered in the literature. Similarly, unlike the PAW pseudopotentials used in the literature, a US pseudopotential was used. Interestingly, the systems *were* successfully modeled at temperatures as high as 500 K, showing smooth convergence in both temperature and pressure. Each carbon isochole successfully relaxed and experienced issues only at high temperatures set in the canonical NVT ensembles. Therefore, the instability likely arises from large, diverging electronic kinetic energies, and resulting pressures, produced during this stage.

As mentioned previously, the computation time required by the simulations placed further limits on the completeness of the results. Due to time constraints, carbon was not simulated at greater temperatures within both a larger representative range of typical WDM (up to 10 million K) and the applicable range of DFT-MD codes (up to 100,000 K). Part of this limitation is attributed to the small time steps needed to model the 24-atom cell. Generally, the larger the system, the less noise present in DFT-MD simulations of WDM. Simpler models, say of 8 or 16 atoms, can be modeled at larger time steps and, as such, enable quicker simulations but also produce larger variation in results. However, this effect is reversed for systems which contain more atoms. In such cases, much smaller time steps, usually on the order of femtoseconds (fs; equal to 10^{-12} s or 10^{-3} ps), are required and were observed in the aforementioned literature. Unfortunately, modeling systems of increasing sizes, say 32, 64, or even 100+ carbon atoms, with such miniscule time steps necessitated greater computing power and resources that were beyond the ability of this work.

Conclusions

The results presented in this work, EOS data of warm dense carbon, do not reproduce those presented in the literature. This work utilized a different procedure – 24-atom cell using Car-Parrinello MD in Quantum ESPRESSO’s *CP* package – than various encountered in the literature used to model such carbon systems. Whether from errors in unit cell setup, errors in the CPMD procedure in QE, or errors from other sources, resulting system pressure does not converge and is shown to be at least 20 to 30 times greater than that accepted in literature for solid carbon in the warm dense range. Furthermore, the results of this work also show the significance of the considerable computational power required by DFT-MD simulations. The calculations executed by DFT-MD software are themselves very complex and, when needed for systems with a large number of atoms, place a substantial burden on processing ability. Not only does increased computational power make quicker execution of simulations and generation of results, but likewise the formation of cause-and-effect relationships between variables and the experimental process as a whole.

Future goals of this research are to design and simulate carbon systems that replicate the results observed in the literature. Although it will continue to modify the 24-atom model introduced here, future work will also utilize the different cells described in the literature. In particular, the carbon system modeled by Bonitz, et al. – a 32-atom cell using Born-Oppenheimer MD in QE’s *PWscf* package – is a fitting candidate. Assuming comparable results are consistently reproduced, further simulations will be carried out to continue the formation of an accurate EOS for carbon in the warm dense region.

Similar DFT-MD simulations for more, increasingly complex elements and substances will develop from the groundwork of simulations of carbon, like those entailed in this work, and other simple systems. Likewise, reliable EOS parameters will enable better, more effective design of materials to be utilized in the warm dense range, particularly those employed in the defense, mitigation, and or handling of nuclear weapons and other highly energetic sources.

Author's Presentations: Conferences

1. Schauss, D. and Miloshevsky, G. *Thermodynamic and Optical Properties of Warm Dense Carbon*. American Physical Society Virtual Meeting, Session J23. Materials in Extremes: Carbon and Related Materials, March 15-19, 2021.

References

- Akbari-Moghanjoughi, M. (2013, April 16). Crystallization and collapse in relativistically degenerate matter. *Physics of Plasmas*, *20*, 042706.
- Ang, S. J., Ser, C. T., & Wong, M. W. (2019). Modeling halogen bonding with planewave density functional theory: Accuracy and challenges. *Journal of Computational Chemistry*, *40*, 1829-1835.
- Benedict, L. X., Driver, K. P., Hamel, S., Militzer, B., Qi, T., Correa, A. A., . . . Schwegler, E. (2014). Multiphase equation of state for carbon addressing high pressures and temperatures. *Physical Review B*, 224109.
- Bonitz, M., Dornheim, D., Moldabekov, Z. A., Zhang, S., Hamann, P., Kählert, H., . . . Vorberger, J. (2020). Ab initio simulation of warm dense matter. *Physics of Plasmas*, *27*, 042710.
- Bussi, G., Donadio, D., & Parrinello, M. (2007). Canonical sampling through velocity-rescaling. *Journal of Chemical Physics*, *126*, 014101.
- Car, R., & Parrinello, M. (1985, November 25). Unified approach for molecular dynamics and density-functional theory. *Physical Review Letters*, *55*(22), 2471-2474.
- Correa, A. A., Bonev, S. A., & Galli, G. (2006, January 31). Carbon under extreme conditions: Phase boundaries and electronic properties from first-principles theory. *PNAS*, *103*(5), 1204-1208.
- Giannozzi, P., Andreussi, O., Brumme, T., Bunau, O., Buongiorno Nardelli, M., Calandra, M., . . . Baroni, S. (2017). Advanced capabilities for materials modelling with Quantum ESPRESSO. *Journal of Physics: Condensed Matter*, 465901.
- Giannozzi, P., Baroni, S., Bonini, N., Calandra, M., Car, R., Cavazzoni, C., . . . Wentzcovitch, R. M. (2009). Quantum ESPRESSO: a modular and open-source software project for quantum simulations of materials. *Journal of Physics: Condensed Matter*, 395502.
- Grumbach, M. P., & Martin, R. M. (1996). Phase diagram of carbon at high pressures and temperatures. *Physical Review B*, *54*(22), 15730-15741.
- Haunschild, R., Barth, A., & French, B. (2019). A comprehensive analysis of the history of DFT based on the bibliometric method RPYS. *Journal of Cheminformatics*, *11*, 72.
- Jacob, C. R., & Neugebauer, J. (2014). Subsystem density-functional theory. *Computational Molecular Science*, *4*, 325-262.
- Kokalj, A. (1999). XCrySDen--a new program for displaying crystalline structures and electron densities. *Journal of Molecular Graphics and Modelling*, *17*, 176-179.
- Kresse, G., & Hafner, J. (1994). Norm-conserving and ultrasoft pseudopotentials for first-row and transition elements. *Journal of Physics: Condensed Matter*, *6*, 8245-8257.

- Kühne, T. D. (2014). Second-generation Car-Parrinello molecular dynamics. *Computational Molecular Science*, 4, 391-406.
- Martinez-Canales, M., Pickard, C. J., & Needs, R. J. (2012, January 27). Thermodynamically stable phases of carbon at multiterapascal pressures. *Physical Review Letters*, 108, 045704.
- Militzer, B., González-Cataldo, F., Zhang, S., Driver, K. P., & Soubiran, F. (2021). First-principles equation of state database for warm dense matter computation. *Physics Review E*, 103, 013203.
- Obot, I. B., Macdonald, D. D., & Gasem, Z. M. (2015). Density functional theory (DFT) as a powerful tool for designing new organic corrosion inhibitors. Part 1: An overview. *Corrosion Science*, 99, 1-30.
- Parrinello, M. (1990). Ab Initio Molecular Dynamics. In F. Yonezawa, *Molecular Dynamics Simulations* (pp. 151-156). Berlin, Heidelberg, Germany: Springer-Verlag.
- Pierson, H. O. (1993). *Handbook of carbon, graphite, diamond, and fullerenes properties, processing, and applications*. Park Ridge, New Jersey, United States of America: Noyes Publications.
- Redmer, R., Nettelmann, N., Holst, B., Kietzmann, A., & French, M. (2008). Quantum molecular dynamics simulations for warm dense matter and applications in astrophysics. In J. Jedrzejewski, *Condensed Matter Physics in the Prime of the 21st Century* (pp. 223-236). London, United Kingdom: World Scientific Publishing Co. Pte. Ltd.
- Singh, D. J. (1994). *Planewaves, pseudopotentials and the LAPW method*. Norwell, Massachusetts, United States of America: Kluwer Academic Publishers.
- Stuart, D. W., & Mosey, N. J. (2020). Pseudodiagonalization-based wavefunction optimization with contracted planewave basis functions. *Journal of Computational Chemistry*, 41, 184-193.
- Zhang, S., Wang, H., Kang, W., Zhang, P., & He, X. T. (2016). Extended application of Kohn-Sham first-principles molecular dynamics method with plane wave approximation at high energy-From cold materials to hot dense plasmas. *Physics of Plasmas*, 23, 042707.

Appendix

Sample input file for ground state relaxation:

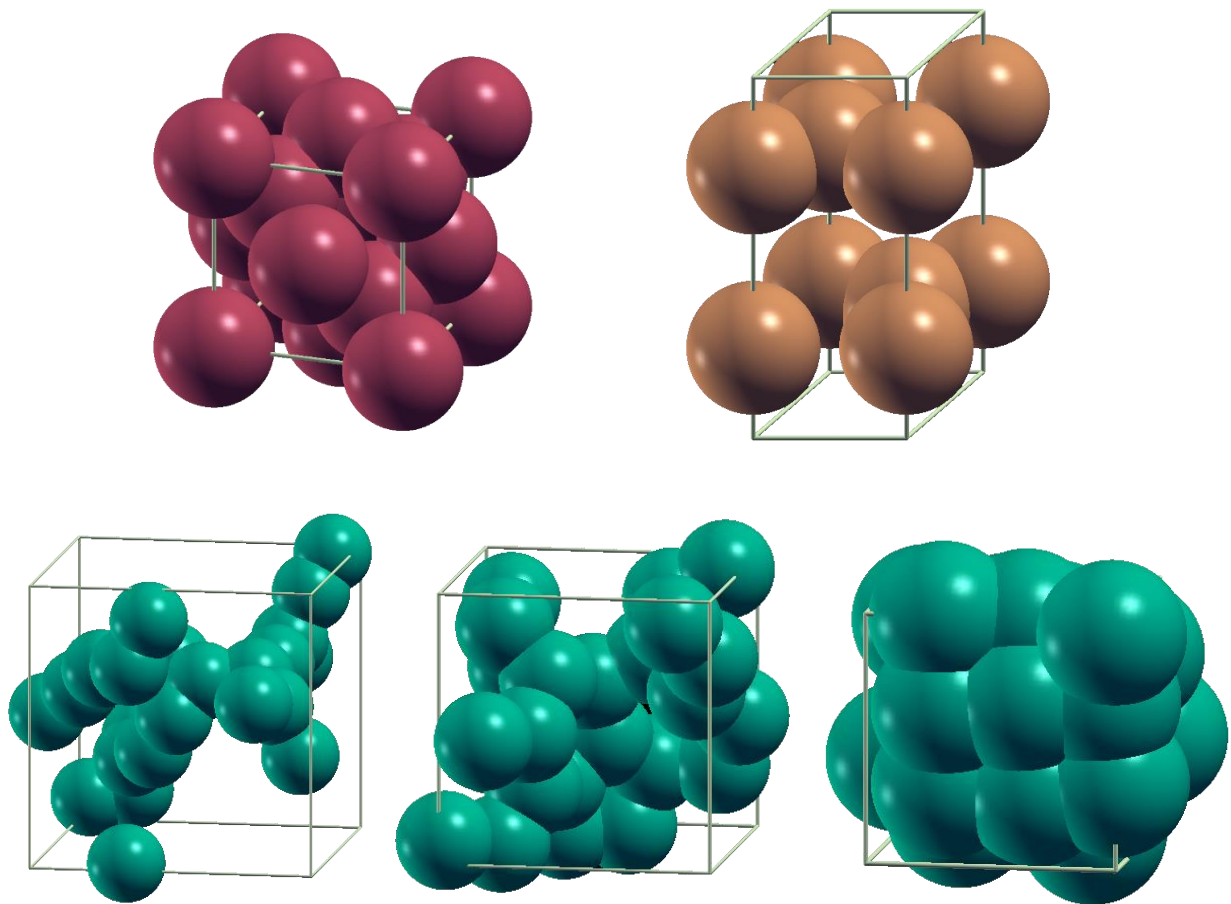
```
# Derek J Schauss
# Equations of State for Warm Dense Carbon from Quantum ESPRESSO
#
# Virginia Commonwealth University
# MS Mechanical and Nuclear Engineering - Graduate Thesis
# via DTRA Grant No. DTRA1-19-1-0019
#
#####
# Step 0 - Electron Ground State Relaxation
# Cell is comprised of 24 carbon atoms assigned random positions
# Time step set sufficiently low enough to enable electron orthogonalization
# Lattice parameter is 14.782... (density of 1.0 g/cc)
#
&CONTROL
  title = 'Carbon Electron Relaxation',
  calculation = 'cp',
  restart_mode = 'restart',
  ndr = 50,
  ndw = 51,
  nstep = 50000,
  iprint = 10,
  isave = 100,
  tstress = .TRUE.,
  tprnfor = .TRUE.,
  dt = 5.0d0,
  etot_conv_thr = 1.0d-9,
  ekin_conv_thr = 1.0d-7,
  prefix = 'C',
  pseudo_dir = './pseudopotentials/',
  outdir = './out/'
/
&SYSTEM
 ibrav = 0,
  celldm(1) = 14.78242,
  nat = 24,
  ntyp = 1,
  ecutwfc = 18.0,
  ecutrho = 216.0,
  nr1b = 10,
  nr2b = 10,
  nr3b = 10
/
&ELECTRONS
  emass = 300.d0,
  emass_cutoff = 2.5d0,
  electron_dynamics = 'sd',
  electron_velocities = 'zero',
  electron_temperature = 'not_controlled'
/
&IONS
  ion_dynamics = 'none',
```

```

        tranp(1) = .FALSE.,
        ion_velocities = 'zero',
        ion_temperature = 'not_controlled'
/
ATOMIC_SPECIES
C 12.011 C.pbe-rrkjus.UPF
ATOMIC_POSITIONS alat
C 0.280356011203167 0.367021423871150 0.455867571703236
C 0.776916976099006 0.765280414054604 0.297958039650056
C 0.676946851594121 0.513295011505302 0.061234084722128
C 0.215082535890976 0.320584711916316 0.398555882769342
C 0.606970164909349 0.658492396428358 0.807595782063456
C 0.317943310664410 0.227495130558507 0.464578409614677
C 0.461762899690624 0.908511069868140 0.092519199795500
C 0.912901986514936 0.381194802707033 0.627956426319524
C 0.071581124549913 0.810918315311952 0.147686651376392
C 0.189392103541370 0.956470220865591 0.041701966115306
C 0.958193366252041 0.714436712042692 0.238590222336978
C 0.905803343249211 0.657343796156498 0.518771923981562
C 0.204823877108311 0.494477333823638 0.088897747003837
C 0.048615394358920 0.073993890211909 0.943099528170713
C 0.086553133178863 0.382447151696649 0.703534312926406
C 0.883729508070553 0.458197731289196 0.673109210203189
C 0.238417298040238 0.683838667051464 0.074207380965819
C 0.528051565911777 0.717464897124428 0.504761115973874
C 0.922369822310433 0.686708382133930 0.218126046993025
C 0.434976004582511 0.575436894076801 0.576627134251442
C 0.140691447446752 0.647416847084907 0.700314067403315
C 0.304339895842419 0.169526164398671 0.909813176343646
C 0.210251179400597 0.799140578151249 0.034574193559873
C 0.126089923272393 0.654274212177481 0.869317392598200
CELL_PARAMETERS alat
    1.0 0.0 0.0
    0.0 1.0 0.0
    0.0 0.0 1.0

```

Hard-sphere unit cell depictions of diamond (top left), graphite, and carbon cells of density 6.0 (bottom left), 8.0 (bottom center), and 10.0 g/cm³:



Relevant parameters for each 24-atom carbon unit cell.

Density (g/cm ³)	Lattice parameter (bohr)	Lattice parameter (Å or 10 ⁻⁸ cm)
1.0	14.78242	7.82256
2.26	11.26443	5.96091
10.0	6.86139	3.63091

Vita

Derek Schauss is a Master's student in the Mechanical and Nuclear Engineering Department. Born and raised in Warrenton, Virginia, he grew up on the Washington Capitals, weekend soccer games, and Christian faith. He attended Kettle Run High School in Nokesville, Va before studying chemical engineering at University of Virginia. During his time in Charlottesville, Derek played club ultimate frisbee, joined Theta Chi fraternity, and worked as both a bouncer and applied mathematics teaching assistant. Prior to enrolling in a graduate program with VCU, Derek labored as an environmental consultant aiding in the design of landfill gas and leachate collection systems. In his free time, he enjoys to read, brew beer, and donate blood.